www.czasopisma.pan.pl PAN POLSKA AKADEMIA NAUK www.journals.pan.pl

jet INTL JOURNAL OF ELECTRONICS AND TELECOMMUNICATIONS, 2020, VOL. 66, NO. 1, PP. 11-16
Manuscript received November 16, 2019; revised January, 2020. DOI: 10.24425/ijet.2019.130259

A Statistical Calibration Method of Propagation Prediction Model Based on Measurement Results

Jan M. Kelner, Michał Kryk, Jerzy Łopatka, and Piotr Gajewski

***Abstract*—Radio environment maps (REMs) are beginning to be an integral part of modern mobile radiocommunication systems and networks, especially for ad-hoc, cognitive, and dynamic spectrum access networks. The REMs will use emerging military systems of tactical communications. The REM is a kind of database used at the stage of planning and management of the radio resources and networks, which considers the geographical features of an area, environmental propagation properties, as well as the parameters of radio network elements and available services. At the REM, for spatial management of network nodes, various methods of propagation modeling for determining the attenuation and capacity of wireless links and radio ranges are used. One method of propagation prediction is based on a numerical solution of the wave equation in a parabolic form, which allows considering, i.a., atmospheric refraction, terrain shape, and soil electrical parameters. However, the determination of a current altitudinal profile of atmospheric refraction may be a problem. If the propagation-prediction model uses a fixed refraction profile, then the calibration of this model based on empirical measurements is required. We propose a methodology for calibrating the analyzed model based on an example empirical research scenario. The paper presents descriptions of the propagation model, test-bed and scenario used in measurements, and obtained signal attenuation results, which are used for the initial calibration of the model.**

***Keywords*—calibration of propagation model, empirical measurements, path loss model, propagation, parabolic equation method, radio environment map**

I. Introduction

PROPAGATION models might be divided into small-, medium- and large -scale models. The small-scale models, also known as channel models, describe propagation phenomena occurring in signals into a small-scale, i.e., primarily fast fading and Doppler effect. The medium-scale and large-scale models describe shadowing, i.e., slow fading, and path loss, i.e., signal attenuation, respectively [1–4]. An example of the separation of propagation-phenomena on the three discussed types of the models is presented in Fig. 1 (based on [4]).

Individual types of propagation models find different applications. In the case of the large-scale models, they are used, i.a., to assess the distance-range of radio systems in various types of environments. Attenuation models may generally be classified into two groups, i.e. statistical and deterministic models. The statistical models illustrating the average path loss in the analyzed propagation environment. In the case of the deterministic models, attenuation for specific points of space can be determined considering landforms, existing buildings, or vegetation, etc. While the statistical models will allow determining the coarse radio range of the analyzed communication system, the deterministic models allow estimating this range depending on a propagation direction. This is schematically illustrated in Fig. 2 (based on [5]) for a hypothetical transmitter (TX).

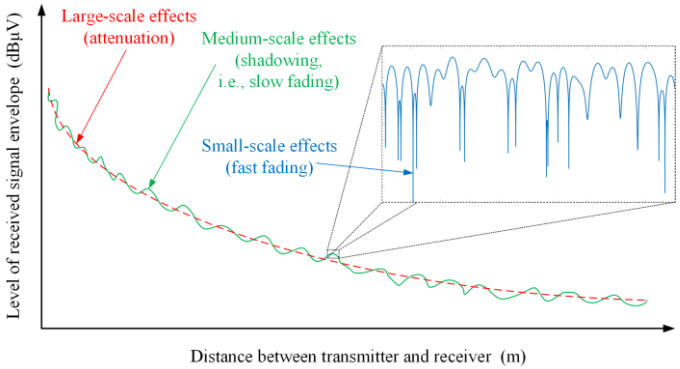

Fig. 1. Separation of propagation phenomena into large-, medium- and small-scale.

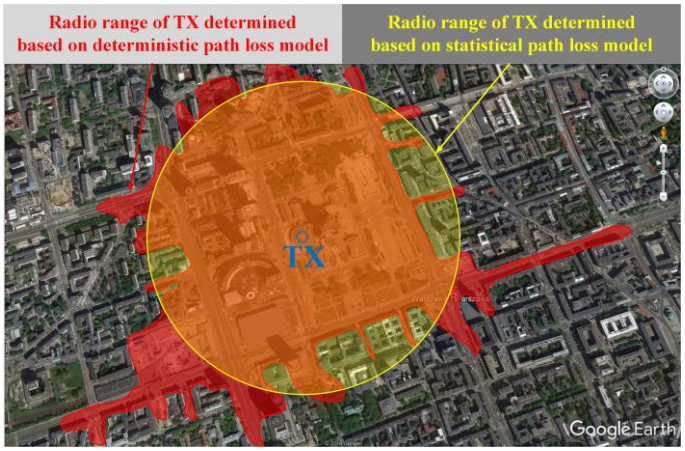

Fig. 2. Example ranges of hypothetical TX determined using statistical and deterministic path loss models.

Jan M. Kelner, Michał Kryk, Jerzy Łopatka, and Piotr Gajewski with the Military University of Technology, Faculty of Electronics, Institute of Communications Systems, Gen. Sylwester Kaliski Str. No. 2, 00-908 Warsaw, Poland (e-mail: jan.kelner@wat.edu.pl, michal.kryk@wat.edu.pl, jerzy.lopatka@wat.edu.pl, piotr.gajewski@wat.edu.pl).

The range evaluation of wireless systems is used for designing radio networks, e.g., in cellar telephony. Then, terrain locations of wireless network nodes, e.g., base stations, is an important issue for providing different services for mobile users, i.e., providing coverage of an area with network access. In the first stage of designing such a network, simulation analyzes are performed in which statistical or deterministic models, e.g., ray-tracing methods [6,7] can be used. In the next approach, measurements are usually made in the real environment.

When planning mobile ad-hoc networks (MANETs), the approach to design the cellular networks cannot be used. On the one hand, the statistical models are too coarse to assess the radio range of MANET nodes. On the other hand, the deterministic ray-tracing methods require a lot of time, high computing power, and accurate spatial digital maps containing information about types of building materials. In addition, it is not possible to perform dedicated propagation measurements due to the dynamically changing situation in such a network. Therefore, different approaches are used in this case. For the radio range assessment, simpler and less accurate deterministic models are usually used than those based on the ray-tracing. In the case of evaluating the real situation between the MANET nodes, results of spectrum sensing [8–13], implemented in modern cognitive networks [14–18] may be utilized. These solutions are used in so-called radio environment maps (REMs) [19–24].

The REM is a kind of database used at the stage of planning and management of the radio resources and networks, which considers the geographical features of an area, environmental propagation properties, as well as the parameters of radio network elements and available services [20,24]. At the REM, for spatial management of network nodes, various methods of propagation modeling for determining the attenuation and capacity of wireless links and radio ranges are used. We propose a propagation prediction method based on a numerical solution of the wave equation in a parabolic form, so-called a parabolic equation method (PEM) [25–28]. The PEM allows considering, i.a., atmospheric refraction, terrain shape, and soil electrical parameters. However, the determination of a current altitudinal profile of atmospheric refraction may be a problem. If the propagation-prediction model uses a fixed refraction profile, then the calibration of this model based on empirical measurements is required. We propose a methodology for calibrating the analyzed model based on an example empirical research scenario. The paper presents descriptions of the propagation model, test-bed and scenario used in measurements, and obtained signal attenuation results, which are used for the initial calibration of the model.

The purpose of this paper is showing the calibration methodology of the propagation prediction model based on sample empirical results. In this case, a path loss model based on the PEM is used to create a propagation awareness in the REM for the needs of planning the MANETs with low antenna-heights of the network nodes.

The remainder of the paper is organized as follows. Section II gives a brief description of the PEM. In Section III, a test-bed, measurement scenario, and obtained empirical results are shown. The calibration methodology of the path loss model based on the PEM is presented in Section IV. The final part of the paper contains a summary.

II. Parabolic Equation Method

The propagation prediction model used to create the REM is based on the PEM, i.e., the numerical solution of the differential parabolic equation for the electric field strength $E(x, z)$ along an assumed azimuth direction (radius), i.e., a corresponding terrain-profile (generalized x coordinate) and for determined height above this terrain (z coordinate) [25,26]

$$\frac{\partial^2 E(x,z)}{\partial z^2} - 2\mathrm{j}k_0 \frac{\partial E(x,z)}{\partial x} + k_0^2 \left(n^2 - 1\right) E(x,z) = 0 \qquad (1)$$

where $\mathrm{j} = \sqrt{-1}$, $k_0 = 2\pi / \lambda$ is a wave number, λ is a wavelength, $n = \sqrt{\mu_r \varepsilon_r}$ is an air refractive index, μ_r and ε_r are relative magnetic and electric permeabilities of air, respectively.

The PEM allows to consider the following physical phenomena [25,26]:

- air refraction, i.e., atmospheric refractivity, and its influence on radio wave propagation;
- terrain diffraction, i.e., radio wave diffraction on a terrain ruggedness, which allows considering the terrain profile in determining the radio range of the TX;
- impact of soil electrical parameters, i.e., ground conductivity and permeability, on wave propagation in a lower part of a troposphere.

Additionally, the proposed solution gives the opportunity to consider the phenomenon of radio wave diffraction in built-up areas. In this case, the height profile of the terrain in a given cross-section should also consider the heights of buildings and other infrastructure [25,26].

In practice, two methods of numerical solution of the parabolic equation are used [25,26], i.e., a finite difference method (FDM) and split-step Fourier method (SSFM). Due to the lower calculation speed of the FDM algorithm, we decided to implement the SSFM method for the PEM solution. In this case, the fast Fourier transform algorithm (FFT) is not implemented in the time and frequency domain, but in the space domain.

The main advantages of the PEM include [25]:

- frequency range of the analysis from 30 MHz to 100 GHz;
- propagation-prediction range from far-field of a transmitting antenna (~1÷30 m) to several hundred kilometers (~300 km);
- considering the terrain profile, i.e., landform, and the radio wave diffraction (terrain diffraction);
- considering the air-refraction phenomena and refractive-index changes along the terrain profile;
- considering the electrical parameters of the soil and their changes along the terrain profile;
- considering a beamwidth of the transmitting antenna in the elevation plane and the vertical or horizontal polarization of the receiving antenna.

The PEM model is used in the REM in two ways. For estimation of the path loss for wireless links, i.e., the point-to-point attenuation between the TX and receiver (RX), and determining propagation attenuation maps around the TXs. These maps are the basis for determining radio-ranges for the individual nodes of the MANET.

Figure 3 shows an exemplary result obtained based on the PEM, i.e., the signal attenuation determined along the analyzed terrain profile and heights above the ground, for a given transmitting antenna hight, h_T. The terrain profiles are determined from digital terrain elevation data (DTED) [29]. The DTED maps are represented by matrices of integers containing information about the ground level measured in meters above mean sea level (AMSL). In this matrix, the desirable terrain profile representing the height component (z coordinate) along the given azimuth direction (generalized x coordinate) should be

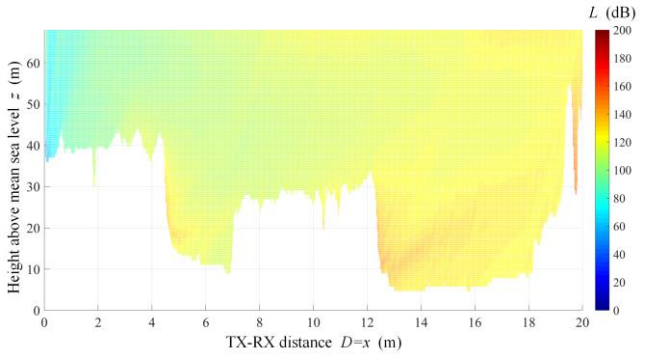

Fig. 3. Sample result of PEM as attenuation distribution for given terrain profile and height of transmitting antenna.

determined. In our analysis, we use DTED2 with a raster resolution of 30 m and we assume h_T = 2 m.

Based on the attenuation distribution, $L(x, z)$, in the XZ plane, where x represents the distance from the TX along the given azimuth direction, while z corresponds to the height, we determine the path loss L for the defined height of the receiving antenna, h_R. Figure 4 depicts the path loss for h_R = 2 m.

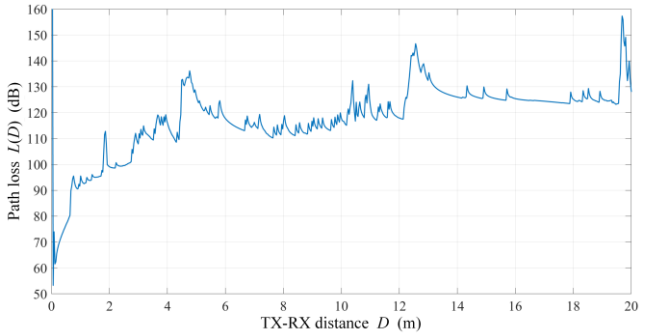

Fig. 4. Sample path loss for given terrain profile and height of receiving antenna.

For the same h_R, we determined the propagation attenuation map illustrated in Fig. 5. This map was generated based on the losses of the paths determined for 360 terrain profiles with a 1° angular step in the azimuth plane. The shown attenuation map corresponds to an area of 40 km × 40 km.

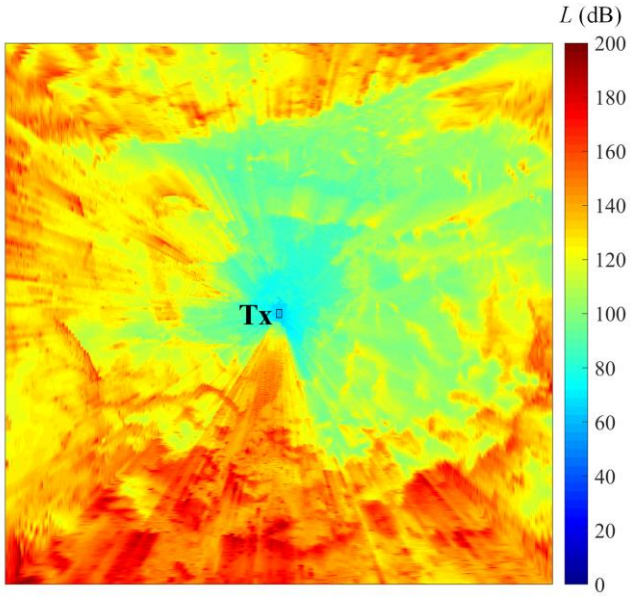

Fig. 5. Exemplary propagation attenuation map for chosen TX and defined height of receiving antenna.

The propagation attenuation map is the basis of the radio range map determined for the individual wireless network nodes (TXs). Figure 6 presents an example of the radio range map obtained for several types of modulation. In this case, detailed information about the TX/RX parameters of the node (e.g., radiated power, antennas gain, noise characteristics of the analyzed modulation and coding schemes, boundary values of signal-to-noise ratio, receiver sensitivity) is required.

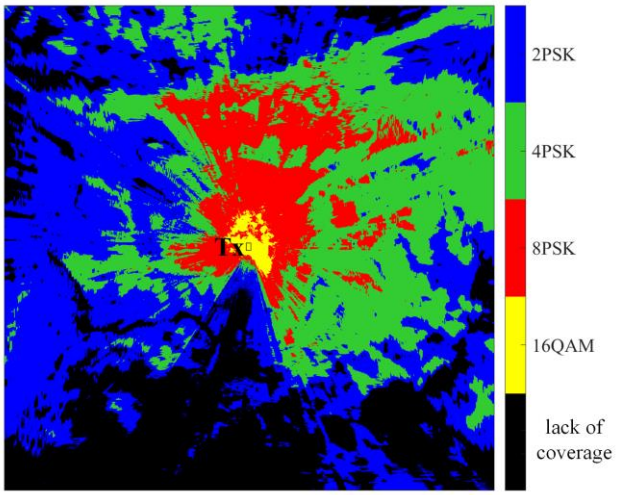

Fig. 6. Exemplary radio range map for chosen TX and defined height of receiving antenna.

III. Empirical Measurements

A. *Measurement test-bed*

To calculate the attenuation correctly from the proposed PEM, the initial calibration should be carried out. Therefore, a measuring campaign was realized to obtain the actual data. The conception of the electromagnetic field strength measurement system is shown in Figs. 7 and 8 for transmitting and receiving parts, respectively.

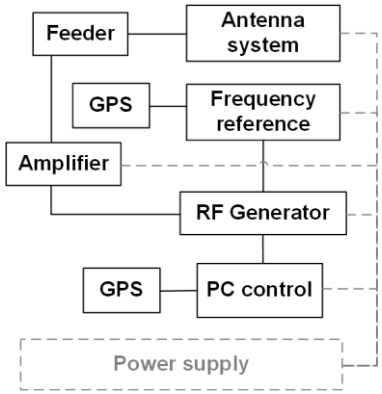

Fig. 7. Block diagram of reference transmitter station.

The reference transmitting station (Fig. 7) is equipped with the signal generator Rohde&Schwarz (R&S) SMIQ02b, which emitted a harmonic signal at a fixed frequency equal to 289.3 MHz. The signal was fed through a 50 W amplifier to an omnidirectional transmitting antenna. The frequency ranges of signal generator, amplifier and antenna are equals 0.3÷2200 MHz, 20÷512 MHz, and 100÷600 MHz, respectively.

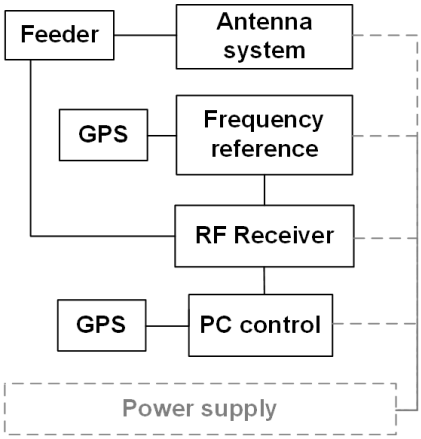

Fig. 8. Block diagram of monitoring station.

During measurements, it was a requirement that the generated signal power was equal to 1 or 10 W. As a result, the signal power level set at the generator was –11 or –5 dBm, respectively.

Both parts of the test-bed can be stationary or mobile. Therefore, scenarios in different places may be proposed. Each of the measurement stations was equipped with a GPS receiver and computer that recorded current time and location.

The main element of the monitoring station (Fig. 8) is the wideband receiver R&S ESMD with a frequency range from 20 MHz to 3.6 GHz. This device was specially developed for signal search, radio monitoring, detection, and spectrum monitoring task.

Fig. 9. Mobile reference transmitter station.

Fig. 10. Mobile monitoring station.

For empirical measurements, the receiver worked in FFM mode with the build-in RMS detector on a 1 kHz frequency range. The receiving antenna used at the monitoring station is the D220R Diamond Antenna and it has a frequency range from 10 to 1600 MHz.

All elements are managed by a computer PC, which enables time and location registration. In addition, it initiates the R&S ESMD and records power levels from detectors.

All stations are installed on mobile platforms that are presented in Figs. 9 and 10.

B. Measurement Scenario

The measurement scenario for the initial calibration of the PEM model was located at the Military University of Technology in Warsaw. A position of the monitoring station (RX) and a movement trajectory of the reference transmitting station (TX) are presented in Figs. 11 (based on [5]) and 12 (based on [30]).

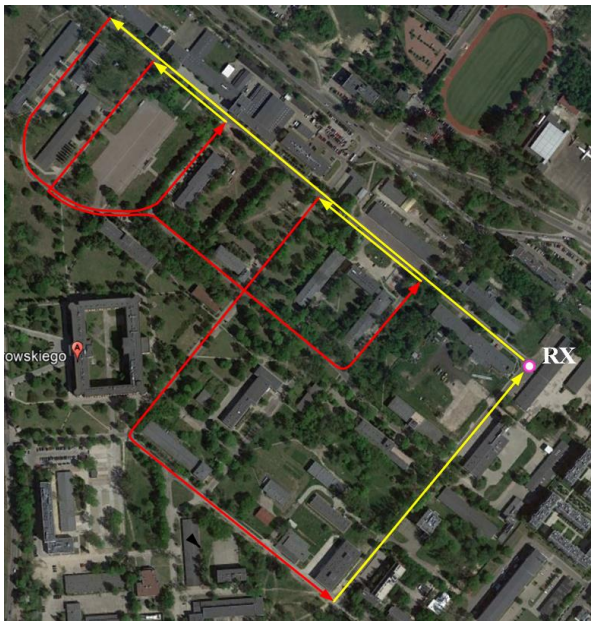

Fig. 11. Empirical measurement scenario.

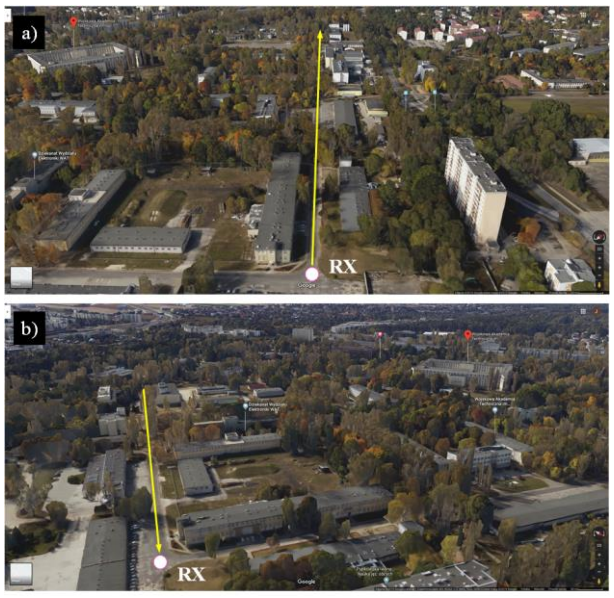

Fig. 12. Spatial placement of initial (a) and final (b) sections of measuring route where LOS conditions occur.

The sections of the TX motion trajectory with line-of-sight (LOS) propagation conditions are marked in yellow. The red lines are means non-LOS conditions between the reference transmitting station (TX) and receiving monitoring (RX) station. We assumed that the RX was stationary and TX was mobile.

C. Measurement Results

During the measurements, log files are created at each station. These files contain information about the system time and current position. Additionally, the received power is recorded in the log file of the monitoring station. After measurements, distance calculation and correlations of both files are required. The results are the relationships between the received power and TX-RX distance or TX movement time.

Figure 13 illustrates the recorded location of both stations. The blue and red lines correspond to LOS and NLOS conditions on the TX movement trajectory, respectively. These results are consistent with the planned scenario depicted in Fig. 11.

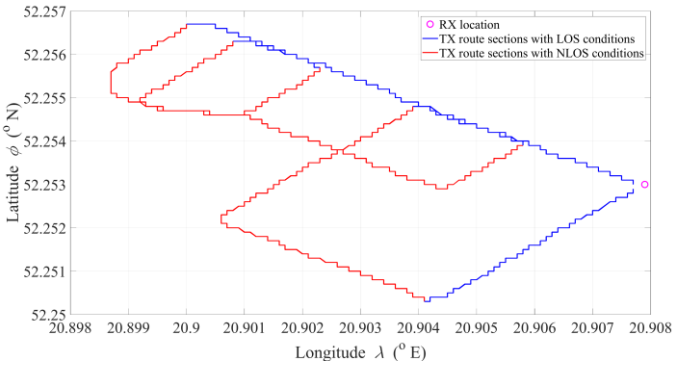

Fig. 13. Monitoring station (RX) location and reference transmitting station (TX) movement trajectory.

The attenuation of the reference signal versus the TX movement time with the region selection for LOS (blue) and NLOS (red) conditions is presented in Fig. 14.

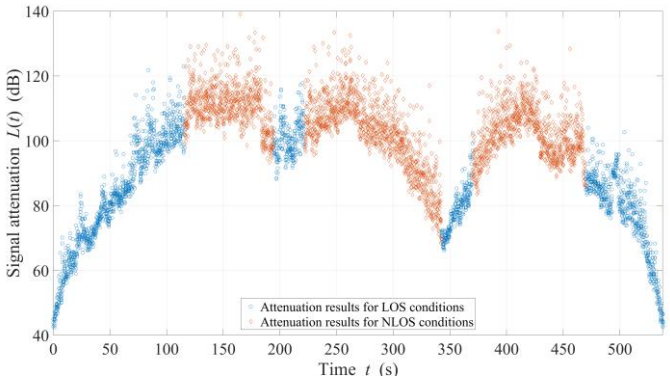

Fig. 14. Attenuation of the reference signal versus TX movement time.

IV. Calibration of Propagation Model

The utilization of the recorded measurement data for the PEM calibration required their preparation. First, we determined the measuring route sections, i.e., signal recording time intervals, corresponding to LOS and NLOS conditions. Next, based on the recorded positions of the transmitting and receiving parts of the test-bed, the distances, D, between the TX and RX were calculated. Finally, by correlating the GPS system times for the data recorded at the transmitting and receiving parts, it was possible to assign the measured attenuations for LOS and NLOS conditions and the distance D. These results are shown in Fig. 15. The data for LOS and NLOS conditions were marked with blue and red, respectively.

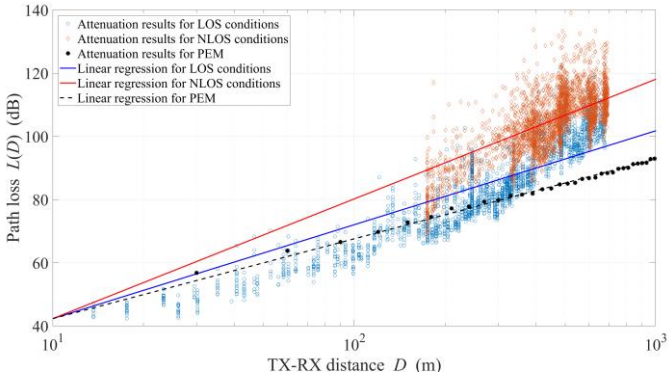

Fig. 15. Empirical path loss models versus TX-RX distance for LOS and NLOS conditions.

For grouped data, we determined empirical close-in free space reference distance path loss (CI) models. The CI model is defined as follows [31–34]:

$$L(D)[\mathrm{dB}] = L(D_0) + n \cdot 10\log_{10}(D/D_0) + X_\sigma \qquad (2)$$

where $L(D_0)$ = 39,6 dB is a free-space path loss (FSPL) for a reference distance equal to D_0 = 10 m, n is a path loss exponent, X_σ is a zero-mean normal random variable with a deviation equal to σ, which represents the shadowing phenomena.

Using the least-squares method [35,36], linear regression was determined for measurement data separately for LOS and NLOS conditions. In these cases, the path loss exponents are n_{LOS} = 2.97 and n_{NLOS} = 3.79, respectively.

Due to the close distances between the TX and RX, and flat terrain, we adopted the flat terrain profile for modeling the analyzed scenario in the PEM. Attenuation was determined for these conditions, which is shown in black in Fig. 15. For the PEM data, the path loss exponent of the CI model is equal to n_{PEM} = 2.53. Therefore, we recommended using correction and calibration factors in the PEM for LOS and NLOS conditions, respectively

$$\Delta n_{LOS} = n_{LOS} - n_{PEM} = 0.44 \qquad (3)$$

$$\Delta n_{NLOS} = n_{NLOS} - n_{PEM} = 1.26 \qquad (4)$$

On their basis, the attenuation $L(D)$ determined in the PEM should be corrected in accordance with the relationship

$$\tilde{L}(D) = L(D) + \Delta n \cdot 10\log_{10}(D/D_0) \qquad (5)$$

where $\Delta n = \Delta n_{\mathrm{LOS}}$ or $\Delta n = \Delta n_{\mathrm{NLOS}}$ for LOS and NLOS conditions, respectively.

V. Conclusions

This paper presents the calibration methodology of the propagation model based on the PEM, which allows considering the terrain diffraction and atmospheric refractivity. The basis for model calibration is empirical data obtained for the described measurement scenario. The presented model calibration was aimed at introducing correction factors for the attenuation determined by the analyzed PEM model separately for LOS and

NLOS conditions. This approach required the separation of measurement data. The presented attenuation correction methodology can also be applied to other propagation prediction models and other measurement scenarios.

The chosen measurement scenario was for the initial PEM model calibration. The current version of the PEM model does not include buildings and vegetations, hence, it is necessary to introduce correction factors for various types of environments, so-called clutters. On the other hand, the PEM model will be used in the REM mainly to assess the radio ranges of the MANET nodes. Therefore, we will ultimately plan to carry out measurement campaigns for significant distances between the TX and RX, in order of 10÷20 km, which will also allow its calibration for such propagation conditions.

REFERENCES

[1] L. W. Barclay, Ed., *Propagation of radiowaves*, 3rd ed. London, UK: The Institution of Engineering and Technology, 2012.

[2] R. Vaughan and J. Bach Andersen, *Channels, propagation and antennas for mobile communications*. London, UK: Institution of Engineering and Technology, 2003.

[3] S. Salous, Radio propagation measurement and channel modelling. Hoboken, NJ, USA: Wiley, 2013.

[4] F. Pérez Fontán and P. Mariño Espiñeira, *Modeling the wireless propagation channel: A simulation approach with Matlab*. Chichester: John Wiley & Sons, 2008.

[5] "Google Earth." [Online]. Available: http://www.google.pl/intl/pl/earth/. [Accessed: 07-Nov-2015].

[6] A. Corucci, P. Usai, A. Monorchio, and G. Manara, "Wireless propagation modeling by using ray-tracing," in *Computational electromagnetics. Recent advances and engineering applications*, R. Mittra, Ed. New York, NY, USA: Springer, 2014, pp. 575–618.

[7] Z. Yun and M. F. Iskander, "Radio propagation modeling and simulation using ray tracing," in *The world of applied electromagnetics. In appreciation of Magdy Fahmy Iskander*, A. Lakhtakia and C. M. Furse, Eds. Cham, Switzerland: Springer, 2018, pp. 275–299.

[8] F. R. Yu, M. Huang, and H. Tang, "Biologically inspired consensus-based spectrum sensing in mobile ad hoc networks with cognitive radios," *IEEE Netw.*, vol. 24, no. 3, pp. 26–30, May 2010. DOI: 10.1109/MNET.2010.5464224.

[9] H. Tang, F. R. Yu, M. Huang, and Z. Li, "Distributed consensus-based security mechanisms in cognitive radio mobile ad hoc networks," *IET Commun.*, vol. 6, no. 8, pp. 974–983, May 2012. DOI: 10.1049/iet-com.2010.0553.

[10] B. Kim, G.-M. Lee, and B.-H. Roh, "ASPD: Adaptive sensing period decision for time-varying channel in military MANETs," in *2014 IEEE Military Communications Conference*, 2014, pp. 643–648. DOI: 10.1109/MILCOM.2014.113.

[11] P. Skokowski, K. Malon, and J. Łopatka, "Properties of centralized cooperative sensing in cognitive radio networks," in *Proceedings of SPIE 10418, 2016 XI Conference on Reconnaissance and Electronic Warfare Systems (CREWS)*, Ołtarzew, Poland, 2017, vol. 10418, p. 1041807. DOI: 10.1117/12.2269996.

[12] K. Malon, P. Skokowski, and J. Łopatka, "Optimization of wireless sensor network deployment for electromagnetic situation monitoring," *Int. J. Microw. Wirel. Technol.*, pp. 1–8, 2018. DOI: 10.1017/S1759078718000211.

[13] M. Kustra, K. Kosmowski, and M. Suchański, "Hybrid sensing method in mobile ad-hoc networks (MANET)," in *2019 20th International Conference on Military Communications and Information Systems (ICMCIS)*, Budva, Montenegro, 2019, pp. 1–8. DOI: 10.1109/ICMCIS.2019.8842695.

[14] J. Mitola and G. Q. Maguire, "Cognitive radio: Making software radios more personal," *IEEE Pers. Commun.*, vol. 6, no. 4, pp. 13–18, Aug. 1999. DOI: 10.1109/98.788210.

[15] S. Haykin, "Cognitive radio: Brain-empowered wireless communications," *IEEE J. Sel. Areas Commun.*, vol. 23, no. 2, pp. 201–220, Feb. 2005. DOI: 10.1109/JSAC.2004.839380.

[16] F. R. Yu, *Cognitive radio mobile ad-hoc networks*. New York, NY, USA: Springer, 2011.

[17] O. Younis, L. Kant, K. Chang, K. Young, and C. Graff, "Cognitive MANET design for mission-critical networks," *IEEE Commun. Mag.*, vol. 47, no. 10, pp. 64–71, Oct. 2009. DOI: 10.1109/MCOM.2009.5273810.

[18] O. Younis *et al.*, "Cognitive tactical network models," *IEEE Commun. Mag.*, vol. 48, no. 10, pp. 70–77, Oct. 2010. DOI: 10.1109/MCOM.2010.5594679.

[19] H. B. Yilmaz, T. Tugcu, F. Alagöz, and S. Bayhan, "Radio environment map as enabler for practical cognitive radio networks," *IEEE Commun. Mag.*, vol. 51, no. 12, pp. 162–169, Dec. 2013. DOI: 10.1109/MCOM.2013.6685772.

[20] M.Pesko, T. Javornik, A. Košir, M. Štular, and M. Mohorčič, "Radio environment maps: The survey of construction methods," *KSII Trans. Internet Inf. Syst.*, vol. 8, no. 11, pp. 3789–3809, Nov. 2014. DOI: 10.3837/tiis.2014.11.008.

[21] P. Bednarek, J. Łopatka, and D. Bicki, "Radio environment map for the cognitive radio network simulator," *Int. J. Electron. Telecommun.*, vol. 64, no. 1, pp. 45–49, Jan. 2018. DOI: 10.24425/118145.

[22] P. Gajewski, "Propagation models in radio environment map design," in *2018 Baltic URSI Symposium (URSI)*, Poznan, Poland, 2018, pp. 234–237. DOI: 10.23919/URSI.2018.8406696.

[23] M. Suchański, P. Kaniewski, J. Romanik, and E. Golan, "Radio environment map to support frequency allocation in military communications systems," in *2018 Baltic URSI Symposium (URSI)*, Poznan, Poland, 2018, pp. 230–233. DOI: 10.23919/URSI.2018.8406717.

[24] M. Suchanski, P. Kaniewski, J. Romanik, E. Golan, and K. Zubel, "Radio environment maps for military cognitive networks: Deployment of sensors vs. map quality," in *2019 19th International Conference on Military Communications and Information Systems (ICMCIS)*, Warsaw, Poland, 2019, pp. 1–6. DOI: 10.1109/ICMCIS.2019.8842720.

[25] M. F. Levy, *Parabolic equation methods for electromagnetic wave propagation*. London, UK: The Institution of Engineering and Technology (IET), 2000.

[26] G. Apaydin and L. Sevgi, *Radio wave propagation and parabolic equation modeling*. Hoboken, NJ, USA: Wiley-IEEE Press, 2017.

[27] K. H. Craig, "Propagation modelling in the troposphere: Parabolic equation method," *Electron. Lett.*, vol. 24, no. 18, pp. 1136–1139, Sep. 1988. DOI: 10.1049/el:19880773.

[28] G. Apaydin and L. Sevgi, "MATLAB-based FEM - parabolic-equation tool for path-loss calculations along multi-mixed-terrain paths," *IEEE Antennas Propag. Mag.*, vol. 56, no. 3, pp. 221–236, Jun. 2014. DOI: 10.1109/MAP.2014.6867720.

[29] National Geospatial-Intelligence Agency (NGA), "Digital Terrain Elevation Data." [Online]. Available: https://www.nga.mil/ProductsServices/TopographicalTerrestrial/Pages/DigitalTerrainElevationData.aspx. [Accessed: 25-Jun-2017].

[30] "Google Maps," *Google Maps*. [Online]. Available: https://www.google.pl/maps/. [Accessed: 30-Jan-2018]

[31] T. S. Rappaport, *Wireless communications: Principles and practice*, 2nd ed. Upper Saddle River, NJ, USA: Prentice Hall, 2002.

[32] T. S. Rappaport, G. R. MacCartney, M. K. Samimi, and S. Sun, "Wideband millimeter-wave propagation measurements and channel models for future wireless communication system design," *IEEE Trans. Commun.*, vol. 63, no. 9, pp. 3029–3056, Sep. 2015. DOI: 10.1109/TCOMM.2015.2434384.

[33] J. M. Kelner and C. Ziółkowski, "Evaluation of angle spread and power balance for design of radio links with directional antennas in multipath environment," *Phys. Commun.*, vol. 32, pp. 242–251, Feb. 2019. DOI: 10.1016/j.phycom.2018.12.005.

[34] F. Qamar, M. N. Hindia, T. Abbas, K. B. Dimyati, and I. S. Amiri, "Investigation of QoS performance evaluation over 5G network for indoor environment at millimeter wave bands," *Int. J. Electron. Telecommun.*, vol. 65, no. 1, pp. 95–101, Feb. 2019. DOI: 10.24425/ijet.2019.126288.

[35] J. R. Taylor, An introduction to error analysis: The study of uncertainties in physical measurements, 2nd ed. Sausalito, Calif: University Science Books, 1997.

[36] P. C. Hansen, V. Pereyra, and G. Scherer, *Least squares data fitting with applications*. Baltimore, MD, USA: Johns Hopkins University Press, 2013